Sea Ice Nonlinearities Act to Rectify and Filter Oceanic and Atmospheric Forcing

BENJAMIN RICHAUD,[a] MICHAEL DOWD,[b] CHRISTOPH RENKL,[a,c] AND ERIC C. J. OLIVER[a]

[a] *Department of Oceanography, Dalhousie University, Halifax, Nova Scotia, Canada*
[b] *Department of Mathematics and Statistics, Dalhousie University, Halifax, Nova Scotia, Canada*
[c] *Physical Oceanography Department, Woods Hole Oceanographic Institution, Woods Hole, Massachusetts*

(Manuscript received 26 August 2024, in final form 26 February 2025, accepted 6 May 2025)

ABSTRACT: The nonlinearities controlling sea ice thermodynamics integrate forcing from the ocean and atmosphere in surprising ways, rendering it difficult to understand the processes affecting sea ice response to climate change. In this study, a simple ice thickness model is forced by realistic stochastic atmospheric and oceanic heat fluxes. Ensemble experiments show that the nonlinearities in the system rectify the added zero-mean noise on weather time scales leading to a change in the mean sea ice state. Most notably, there is a thinning in summer when sea ice is already at its minimum. The sea ice system integrates high-frequency forcing to influence longer time scales, thus changing not only the mean state but also the interannual-to-decadal variability of sea ice. Adding a trend to the forcing variables yields estimates of the dominant drivers of the current and future ice loss in the Arctic, with a prevalent role of ice–ocean heat flux over surface heat fluxes. This study reveals sea ice as a fundamental climate component, absorbing the energy into its mean state and transforming weather fluctuations with time scales of days to weeks into internal variability on time scales of months to decades.

SIGNIFICANCE STATEMENT: Understanding how sea ice responds to changes in the Arctic climate is crucial to predict its future. Using a simple model, ice thickness is shown to react in unexpected ways to small changes in atmospheric and oceanic conditions. Sea ice absorbs parts of those changes to modify its average thickness and transforms short-term weather fluctuations (lasting days to weeks) into longer-term changes in ice thickness (lasting months to decades). When it comes to Arctic warming, trends in the atmosphere and ocean have different impacts on the ice melt. The ocean plays a bigger role in determining when a seasonally ice-free Arctic will occur. This study emphasizes that sea ice is a key part of the climate system.

KEYWORDS: Ocean; Arctic; Stochastic models; Interannual variability; Internal variability

1. Introduction

The rapid changes of the Arctic environment in the context of accelerating anthropogenic climate change have led to the proclamation of "The New Arctic Ocean" (Weingartner et al. 2022). The Arctic is warming at 4 times the rate of the global average (Rantanen et al. 2022), September sea ice extent has declined by 12.7% per decade over 1979–2021, and ice more than 4 years old has virtually disappeared (Meier and Stroeve 2022), with consequences on biogeochemical cycling (e.g., Lannuzel et al. 2020; DeGrandpre et al. 2020; Duke et al. 2023), ecosystems (e.g., Arrigo and van Dijken 2011; Boetius et al. 2013; Ardyna and Arrigo 2020), and Indigenous peoples (Cunsolo Willox et al. 2013a,b; Middleton et al. 2020a,b).

The main source of uncertainty for estimating the trend of declining sea ice extent is the internal variability of sea ice (Swart et al. 2015; Holland and Hunke 2022). Internal variability, the variation of the mean and other statistical moments of a system under constant or periodic external forcing, is intrinsic to the system and can typically arise from feedbacks that destabilize the system (e.g., IPCC 2021). Numerous feedback mechanisms occur in the ice system that can generate such internal variability (Goosse et al. 2018). The positive albedo feedback is related to the change in albedo, the proportion of shortwave radiation reflected back into the atmosphere (Meehl and Washington 1990). Snow and cold ice have a high albedo, while melt ponds have a low albedo, increasing the proportion of shortwave radiation absorbed by the ice, leading to more melt and further lowering the albedo (Perovich and Polashenski 2012; Light et al. 2022). Another important feedback mechanism regulating the ice variability is the negative, stabilizing ice growth–thickness feedback, related to the thermodynamics of sea ice: a thin layer of ice conducts heat more efficiently, leading to stronger cooling at the ice–ocean interface if the atmosphere is cold enough, and more basal ice formation (Bitz and Roe 2004). This feedback is tied to the mean state of the ice (defined as the annual mean sea ice volume north of 80°N) and, along with the albedo feedback, is critical to assess sea ice changes and to reduce ice thickness biases in numerical simulations (Massonnet et al. 2018).

An approach to understanding internal climate variability was provided by Hasselmann (1976), using stochastic climate

Supplemental information related to this paper is available at the Journals Online website: https://doi.org/10.1175/JCLI-D-24-0485.s1.

Richaud's current affiliation: Université Catholique de Louvain, Louvain-la-Neuve, Belgium.

Corresponding author: Benjamin Richaud, benjamin.richaud@uclouvain.be

DOI: 10.1175/JCLI-D-24-0485.1

models. It was demonstrated that the stochastic, rapidly fluctuating white noise of atmospheric weather is integrated by the climate system components into slowly varying red noise of climate variability. This theoretical framework was successfully applied to a variety of systems and time scales to explain changes in sea surface temperature on times scales of months to years (Frankignoul and Hasselmann 1977), as well as the dynamics of Arctic and Antarctic sea ice cover (Lemke et al. 1980), the Atlantic Ocean subseasonal-to-seasonal (Renkl et al. 2024) and multidecadal variability (Liu et al. 2023). It was deemed influential enough to be worthy of the 2021 Nobel Prize, awarded to Klaus Hasselmann. The concept has been expanded to double integrations, meaning systems where one variable is integrated as a forcing to a second variable, which is then further integrated as a forcing to a third variable, to explain variations on even longer time scales (e.g., Kilpatrick et al. 2011; Di Lorenzo and Ohman 2013). The sea ice climate component sits at the interface between the atmosphere and the ocean and is therefore subject to heat flux forcing at its upper and lower boundaries. Following the stochastic climate framework, the atmospheric forcing can be treated as a near white weather noise, while the oceanic forcing is a more slowly evolving red noise. How will sea ice thickness respond to both forcings, merging different time scales? Under what circumstances will the rapid atmospheric stochastic noise dominate relative to the slower oceanic stochastic noise? It is also unknown when and how both stochastic forcings will act together, and how the rapidly evolving Arctic could impact the internal variability of the sea ice system.

The response to variability in the forcing of nonlinear climate systems is of significant interest in the context of climate change. Nonlinear systems can accumulate small, high-frequency variations, transferring the energy into a mean-state change. This process is called a rectification (as taken from the electrical rectifier). For example, seasonal sea ice cover can lead to an increased annual oceanic carbon uptake by preventing outgassing in winter while allowing uptake when biological or chemical processes lower surface CO_2 partial pressure, mechanisms coined the "rectification" hypothesis (Yager et al. 1995) and the sea ice carbon pump (Rysgaard et al. 2011; Richaud et al. 2023). Increased variance can also lead the system to cross bifurcation points, the thresholds necessary to jump from one equilibrium state into the next (e.g., Lenton et al. 2008; Wagner and Eisenman 2015; Ditlevsen and Ditlevsen 2023). The sea ice extent, with the rapid ice loss events of 2007 and 2012 in the Arctic, and more recently in 2017, 2022, and 2023 around Antarctica, is exhibiting this increased variability, leading to discussions about the potential for a tipping point related to ice processes (Serreze and Francis 2006; Holland et al. 2006; Eisenman and Wettlaufer 2009). Several studies have investigated stochastic equations of a simple enthalpy model combining ice and upper ocean to study the stability of the ice system and the influence of statistical noise on the system (Flato and Brown 1996; Moon and Wettlaufer 2011, 2013, 2017; Wagner and Eisenman 2015), but without including the influence of a variable ice–ocean heat flux. Other studies including a variable oceanic heat source have highlighted that an increase in ocean heat transport into the Arctic can trigger abrupt sea ice retreats (Holland et al. 2006; Merryfield et al. 2008).

In this study, we use a simple sea ice model to investigate the nonlinear responses of sea ice thickness to stochastic forcing, including impacts on its mean state, variability, and trends. In particular, the role of the ice–ocean heat flux, often neglected in stand-alone ice models, needs better understanding. We examine how a change in the variability or the trend of atmospheric and ice–ocean heat fluxes consistent with anthropogenic climate change could impact ice thickness in the Arctic Ocean. A description of the sea ice model is first provided, including the expected nonlinearities of the system (section 2a). The stochastic forcing, capturing weather timescale fluctuations, is idealized but realistic, using parameters constrained by reanalysis data for the atmospheric forcing and model outputs and in situ observations for the oceanic forcing (section 2b). The model inputs are generated using statistical methods (section 2c). The introduction of stochastic noise in the forcing leads to a nonlinear response, impacting the mean state of sea ice toward lower values and inducing a low-frequency variability (section 3a). While the model is particularly sensitive to atmospheric noise in its nonlinear response, the increasing trend of the ice–ocean heat flux dictates the fate of summer ice (section 3b). Finally, we discuss the limitations of this study and the implications of the results for the variability and future of the Arctic sea ice cover, including a proposed inverse energy cascade perspective for ice thickness (section 4).

2. Model and methods

The evolution of ice models has been mostly guided by the perspective of quantitatively reliable climate models aimed at demonstrating predictive skill. In this study, we focus on a process-oriented thermodynamic understanding. We rely on the simple, zero-layer ice model derived by Semtner (1976), as it provides a qualitatively satisfying simulation of ice thickness. We discuss the limitations of this simple model in the discussion section.

a. Sea ice model

The model is based on heat flux balances at the surface and bottom of a slab of ice of thickness H_i (m, with i standing for ice), with surface temperature (at the ice–atmosphere interface) T_s and bottom temperature (ice–ocean interface) T_b (K; see Fig. 1). We assume that there is no snow on top of the ice. Within this single slab of ice, the temperature gradient is assumed to be linear. The vertical heat conduction inside the ice is then,

$$F_{c,i} = -k_i \frac{\partial T}{\partial z} = -k_i \frac{T_s - T_b}{H_i}, \tag{1}$$

with the heat conductivity k_i (W m^{-1} K^{-1}) considered constant (see Table 1 for symbols and standard values of the main parameters used in this study). The vertical axis z is positive upward, with its origin fixed at the ice–atmosphere interface (Fig. 1). Following this convention, the heat flux $F_{c,i}$ is also positive upward.

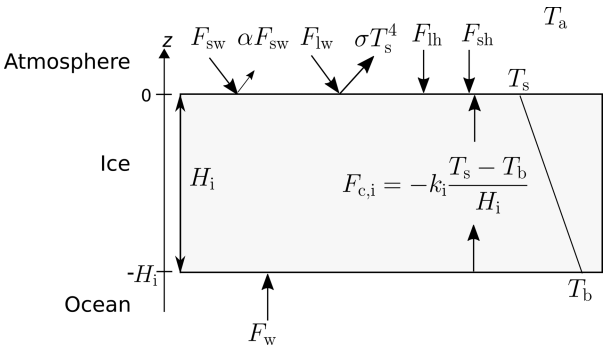

FIG. 1. Schematic of the ice model variables and forcing. The F_{sw} is the downward shortwave radiation, αF_{sw} is the fraction of incident shortwave radiation reflected upward (with α the surface albedo), F_{lw} is the downward longwave radiation, σT_s^4 is the upward longwave radiation emitted by the ice (following the Stefan–Boltzmann law), F_{lh} is the latent heat flux due to sublimation and deposition, F_{sh} is the atmospheric sensible heat flux, $F_{c,i}$ is the vertical heat conduction inside the ice, and F_w is the oceanic sensible heat flux. The T_a is the atmospheric temperature, T_s is the ice surface temperature, and T_b is the ice bottom temperature. The H_i is the ice thickness, and k_i is the heat conductivity in the ice. See text and Table 1 for more details.

A heat balance is imposed for the bottom interface. The incoming sensible heat flux F_w (W m^{-2}, positive upward) between the ice and the ocean is partially balanced by the heat conduction. The remaining heat can only be dissipated by a latent heat flux, leading to ice growth or melt:

$$L_i \left.\frac{dH_i}{dt}\right|_{\text{bot}} = F_{c,i} - F_w, \tag{2}$$

where L_i is the constant latent heat capacity (J m^{-3}) and $dH_i/dt|_{\text{bot}}$ is the ice growth rate (m s^{-1}) at the bottom ($z = H_i$). If $T_s < T_b$, the heat conduction exports heat from the bottom to the surface, leading to ice growth if the heat conduction is larger than the ice–ocean heat flux. On the other hand, if $T_s > T_b$, the heat conduction is negative, leading to ice melt; ice melt at the bottom also occurs if the ice–ocean heat flux F_w is larger than the conductive heat flux $F_{c,i}$, regardless of the surface temperature.

Another heat balance is used at the ice–atmosphere interface, but with an important difference: at the surface, ice cannot grow since there is no water to freeze. If the surface temperature T_s is below the melting point (273.15 K = 0°C), the conductive heat flux $F_{c,i}$ is entirely balanced by the net atmospheric heat fluxes F_s (W m^{-2}, positive downward, in contrast to the other heat fluxes) so that

$$F_{c,i} + F_s = 0. \tag{3}$$

If T_s reaches the melting point, it cannot go higher, and the excess heat is then converted into a latent heat flux of melting. The ice growth rate at the surface ($z = 0$) can then be written as

$$L_i \left.\frac{dH_i}{dt}\right|_{\text{surf}} = \begin{cases} 0, & \text{if } T_s < 273.15 \text{ K} \\ -F_s - F_{c,i}, & \text{if } T_s = 273.15 \text{ K} \end{cases}. \tag{4}$$

The total ice growth rate is given by the sum of the growth rates at the surface and the bottom. Both heat balance (2) and (4) can then be combined to give

$$L_i \frac{dH_i}{dt} = L_i \left.\frac{dH_i}{dt}\right|_{\text{surf}} + L_i \left.\frac{dH_i}{dt}\right|_{\text{bot}} = \begin{cases} -k_i \dfrac{T_s - T_b}{H_i} - F_w, & \text{if } T_s < 273.15 \text{ K} \\ -F_s - F_w, & \text{if } T_s = 273.15 \text{ K} \end{cases}. \tag{5}$$

In this formulation, H_i is the model variable, F_w and F_s are forcing variables, L_i and k_i are model parameters, and T_s and T_b are model diagnostic variables. The bottom temperature T_b is considered to be constant at the freezing point of seawater (following Maykut and Untersteiner 1971; Semtner 1976).

The net surface heat flux F_s includes longwave (thermal) and shortwave (solar) radiation, and sensible and latent heat fluxes (Fig. 1). The net longwave radiation can then be written as $F_{lw} - \sigma T_s^4$, with F_{lw} representing the downward longwave radiation emitted by the atmosphere and $-\sigma T_s^4$ representing the upward radiation emitted by the ice surface following the Stefan–Boltzmann law (Maykut and Untersteiner 1971). The net shortwave radiation takes into account that a fraction is reflected due to the albedo α of the ice and is therefore $(1 - \alpha)F_{sw}$ at the top of the ice. The ice albedo depends on a number of parameters. We take a simple approach by assuming the albedo to vary between two states to reflect the increased presence of melt ponds and bare ice when the surface temperature reaches the melting point (Perovich and Polashenski 2012):

$$\alpha = \begin{cases} \alpha_i, & \text{if } T_s < 273.15 \text{ K} \\ \alpha_m, & \text{if } T_s = 273.15 \text{ K} \end{cases}, \tag{6}$$

with $\alpha_i > \alpha_m$ (see Table 1). The latent heat flux at the surface F_{lh} only includes the latent heat due to sublimation (evaporation of ice) and deposition (condensation of water vapor) since the melting of sea ice is already included in (5). Finally the sensible heat flux at the ice surface F_{sh} is parameterized as

$$F_{sh} = \rho_a c_{p,a} c_{sh} U_{wd} (T_a - T_s) = f_{sh}(U_{wd})(T_a - T_s), \tag{7}$$

with $f_{sh}(U_{wd}) = \rho_a c_{p,a} c_{sh} U_{wd}$ representing a transfer function of the wind speed U_{wd} at 10 m, ρ_a representing the air density, $c_{p,a}$ representing the air specific heat capacity, c_{sh} representing a transfer coefficient, and T_a representing the atmospheric temperature at 2 m. The net surface heat flux can then be written as

$$F_s = (1 - \alpha)F_{sw} + F_{lw} - \sigma T_s^4 + f_{sh}(U_{wd})(T_a - T_s) + F_{lh}. \tag{8}$$

For the case when the surface temperature is below melting, (3) and (8) provide a fourth-order polynomial for T_s:

$$\sigma T_s^4 + \left[f_{sh}(U_{wd}) + \frac{k_i}{H_i} \right] T_s - \left[(1 - \alpha)F_{sw} + F_{lw} + f_{sh}(U_{wd})T_a + F_{lh} + \frac{k_i T_b}{H_i} \right] = 0, \tag{9}$$

TABLE 1. Model parameters. When the parameters vary between ice states, the three values are indicated for the seasonal (72°N), thin perennial (75°N), and thick perennial (85°N) ice states.

Symbol	Brief description	Standard value 72°N	Standard value 75°N	Standard value 85°N	Units	Range (sensitivity experiments)	Source
	Model variables						
H_i	Ice thickness (prognostic variable)				m		
T_s	Sea ice surface temperature				K (or °C)		
	Forcing variables						
F_{lw}	Downward longwave (thermal) radiation				W m^{-2}		ERA5
F_{sw}	Downward shortwave (solar) radiation				W m^{-2}		ERA5
F_{sh}	Atmospheric sensible heat flux [(7)]				W m^{-2}		ERA5
F_{lh}	Atmospheric latent heat flux				W m^{-2}		ERA5
F_w	Ice–ocean sensible heat flux				W m^{-2}		NAPA model and ITPs
T_a	Atmospheric temperature at 2 m				K		ERA5
	Forcing parameters						
ρ_a	Atmospheric density		1.22		kg m^{-3}		Goosse (1998)
$c_{p,a}$	Atmospheric specific heat capacity		1005		J kg^{-1} K^{-1}		Goosse (1998)
c_{sh}	Ice–atmosphere sensible heat transfer coefficient		1.75×10^{-3}		—		Goosse (1998)
U_{wd}	Atmospheric wind speed at 10 m	6.2	5.8	5.8	m s^{-1}		ERA5
σ	Stefan–Boltzmann constant		5.67×10^{-8}		W m^{-2} K^{-4}		Maykut (1986)
	Thermodynamic model parameters						
α_i	Solid ice albedo (when $T_s < T_m$)		0.8		—	0.4–0.8	Perovich and Polashenski (2012)
α_m	Melt albedo (when $T_s = T_m$)		0.5		—	0.1–0.7	Perovich and Polashenski (2012)
k_i	Sea ice heat conductivity		2.3		W m^{-2} K^{-1}	2.0–3.2	Weeks and Hibler (2010)
L_i	Sea ice specific latent heat of fusion		300×10^6		J m^{-3}	150–335 ($\times 10^6$)	Semtner (1976)
T_b	Ice temperature at ice–ocean interface		271.40 (−1.75)		K (°C)		
T_m	Melting point of sea ice		273.15 (0)		K (°C)		
	Statistical model parameters						
$\varphi_{1\mathrm{w}}$	AR(1) longwave parameter (time scale)		0.7 (3.3)		— (days)		ERA5
φ_{sw}	AR(1) shortwave parameter (time scale)		0.6 (2.5)		— (days)		ERA5
φ_{T_a}	AR(1) temperature parameter (time scale)		0.85 (6.6)		— (days)		ERA5
$\varphi^1_{F_w}$	AR(2) F_W parameter 1 (time scale)		0.75 (4)		— (days)		NAPA model
$\varphi^2_{F_w}$	AR(2) F_W parameter 2 (time scale)		0.55 (25)		— (days)		NAPA model
ρ_{12}	Cross correlation, $F^{\mathrm{NRes}}_{\mathrm{lw}}$, and $F^{\mathrm{NRes}}_{T_a}$	0.64	0.73	0.73	—		ERA5
ρ_{13}	Cross correlation, $F^{\mathrm{NRes}}_{\mathrm{lw}}$, and $F^{\mathrm{NRes}}_{\mathrm{sw}}$	−0.64	−0.64	−0.59	—		ERA5
ρ_{23}	Cross correlation, $F^{\mathrm{NRes}}_{T_a}$, and $F^{\mathrm{NRes}}_{\mathrm{sw}}$	−0.22	−0.33	−0.27	—		ERA5

which has only one physical root. It can then be solved to calculate T_s and close (5). If the solution is above the melting point, T_s is constrained to 273.15 K and used to close (8) and (5).

The model is solved numerically using the Python language.[1] We inject discrete-time stochasticity in the forcing via multivariate autoregressive models (see section 2c below), interpolated on the model time step, then calculate the surface temperature via (9) and finally solve (5). The model is integrated with a solver based on an implicit Runge–Kutta scheme, of order 5(4), implemented in the SciPy Python library. The time step is variable to optimize convergence time and accuracy, but it is set to not exceed 8 h. The model results are insensitive to the maximum time step or to the numerical scheme implemented (not shown).

A few results can already be anticipated by analyzing the equations of this model. The conditional expression of (5) has mathematical consequences. If the surface temperature is at the melting point, the ice thickness follows a first-order linear differential equation of the form $dH_i/dt = F_0(t)$, with $F_0(t)$ representing a forcing term independent of H_i. If the surface temperature is below the melting point, then the ice thickness follows a nonlinear differential equation of the form $dH_i/dt = F_1(t)(1/H_i) + F_2(t)$, with $F_1(t)$ and $F_2(t)$ forcing terms. While $F_2(t)$ is independent of H_i, $F_1(t)$ is a function of T_s which depends on H_i. Moreover, the switch from one state to the other depends on T_s, which is once again dependent on H_i. This model is therefore partially nonlinear with H_i on various

[1] The code is publicly available, see Data Availability statement.

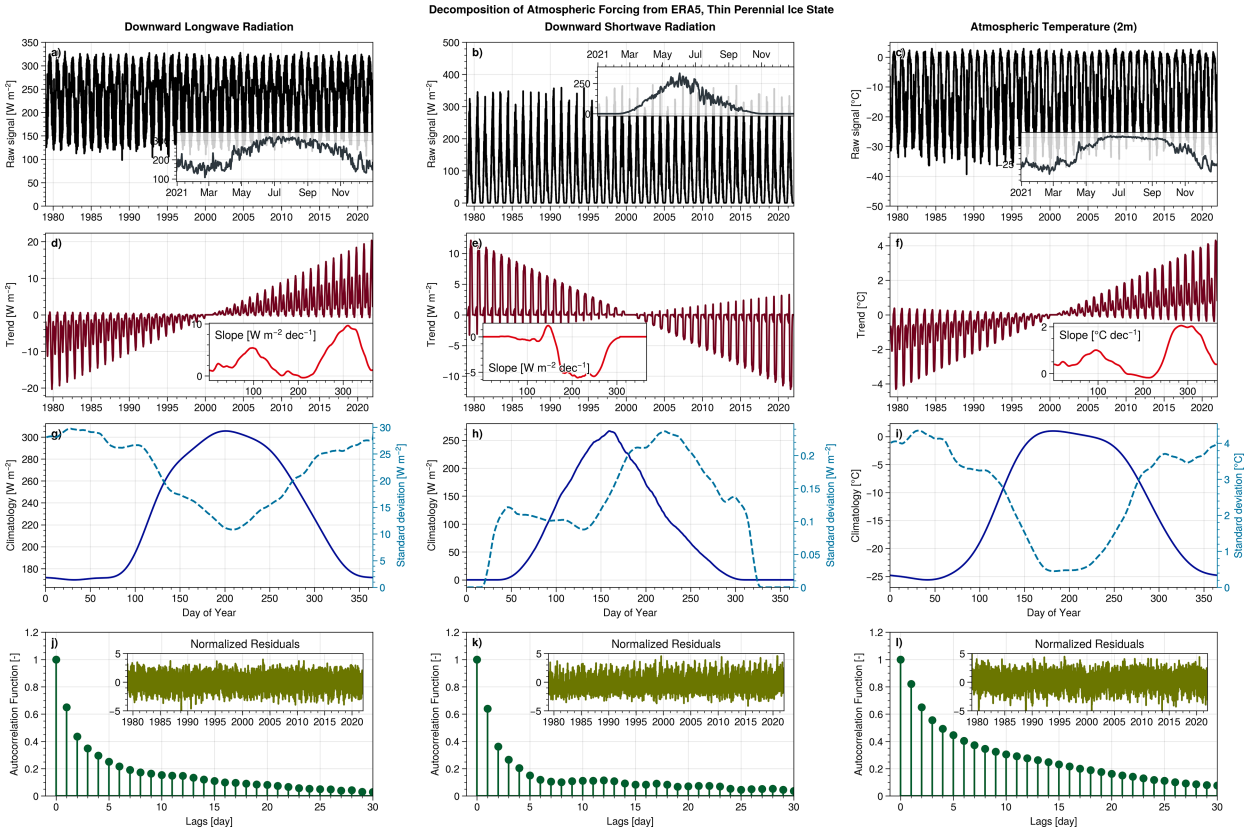

FIG. 2. Decomposition of ERA5 (a) downward longwave and (b) shortwave radiations and (c) atmospheric temperatures from 1979 to 2021 (insets show 2021) into (d)–(f) trends (with day-of-year slopes in inset), (g)–(i) seasonal cycle (solid line) and standard deviation (dashed blue line), and in (j)–(l) normalized residuals (insets) with the associated autocorrelation function. The normalized residuals of shortwave radiation [inset in (k)] still exhibit some seasonality due to the polar night. This decomposition is here illustrated for the thin perennial ice state (75°N, 210°E).

levels. The conditional expression acts as a rectifier for the atmospheric forcing, including it directly into the melting rate when the surface temperature is at the melting point, but discarding it during the growing phase; the opposite is also true for the conductive heat flux inside the ice. This is likely to lead to transfer of any variability into the mean ice state, as described earlier (section 1).

Our model formulation, with the two-state albedo [(6)] and the inverse dependence on H_i in the heat conduction [(1)], allows for two well-known mechanisms to exist: the positive albedo feedback and the ice growth–thickness feedback. It is not trivial to anticipate how those nonlinearities will integrate atmospheric and oceanic forcing, in particular if they contain a stochastic component.

b. *Forcing data*

The model is forced using simulated but realistic forcing. To elucidate the sensitivity of sea ice to different components of the meteorological and oceanographic conditions, the forcing is decomposed into three components: the trend, the climatology, and the short time-scale noise (also called weather noise). The general approach is to define the trend and climatology empirically from data in such a way that the remaining residuals are stationary and can be modeled as a simple stochastic process. The trend, climatology, and weather noise parameters can then be altered to simulate a wide range of past, present, and future Arctic conditions, and ensemble runs with different stochastic realizations of the noise provide statistical robustness to the results. The fifth major global reanalysis produced by ECMWF (ERA5; Hersbach et al. 2020) product was used to decompose atmospheric forcing (Fig. 2). Three representative grid cells have been extracted at longitude 210° and three latitudes covering the Beaufort Gyre. Those latitudes were chosen to provide different representative ice conditions: seasonal (72°N), perennial with thin summer ice (75°N), and perennial with thick summer ice (85°N). While the incoming downward longwave and shortwave radiation F_{lw} and F_{sw} at the surface are directly taken from ERA5 (Figs. 2a,b), the sensible heat flux depends on ice conditions and needs to be calculated via (7), using wind speed U_{wd} and atmospheric temperature T_a (Fig. 2c). We use constant wind speeds calculated as the annual average from ERA5 (Table 1), as they are relatively constant through time in the Arctic (Spreen et al. 2011; Vavrus and Alkama 2022), and sensitivity experiments found the thermodynamic model to be insensitive to wind speed variations (not shown). The model was also found to

not be very sensitive to latent heat flux variability (not shown) so this component is imposed as a climatology, estimated from ERA5 data.

A smoothed trend is calculated for each day of the year to account for the strong seasonality of the forcing variables (Figs. 2d–f; for technical details, see supplemental information S1 in the online supplemental material; for decomposition of the other latitudes, see Figs. S4 and S5). Once the trend is removed, a smoothed climatology representing the seasonal cycle is determined (Figs. 2g–i, solid line). The remaining residuals still exhibit a strong seasonally varying variance and are therefore not stationary. Seasonally varying standard deviations σ_{lw}, σ_{T_a} and σ_{sw} are calculated and used to normalize the residuals (Figs. 2g–i, dashed line). The autocorrelation functions of the normalized residuals show a relatively rapid decay and little other structure (Figs. 2j–l). It can therefore be fit with an autoregressive (AR) model of order 1 (see below and Table 1 for values). This can be used to generate stochastic residuals.

The ice–ocean sensible heat flux F_w is difficult to constrain due to the limited availability of observations. Most of the previous studies using stand-alone models tend to apply a constant ice–ocean heat flux, often 2 W m^{-2} (e.g., Maykut and Untersteiner 1971; Semtner 1976; Wagner and Eisenman 2015). Yet, F_w exhibits a strong seasonality and trend. To evaluate realistic parameters for F_w, we use ice-tethered profiler (ITP) observations (Toole et al. 2011), as well as a regional ice–ocean numerical model covering the Arctic (Zhang et al. 2020; see SI for more details on the model). By combining both sources and comparing them to the available scientific literature (Maykut and McPhee 1995; Krishfield and Perovich 2005; McPhee 2008), a reasonable estimate of the climatology and variance can be determined (supplemental information S1). The seasonal cycle of the modeled ice–ocean heat flux shows a stable, small heat flux in winter, with values around 2 W m^{-2} from October to May, and a significant increase to a peak of around 30 W m^{-2} in mid-August (Fig. S1), consistent with ITP temperatures and with the same literature noted above. Superimposed on the seasonal cycle, large variations occur, especially in summer, with values up to 100 W m^{-2}, once again consistent with the previously provided scientific literature. Once the climatology is removed, the residuals exhibit a large seasonally varying standard deviation σ_{F_w}. These follow the same temporal pattern as the climatology with values going from 1 W m^{-2} in winter to above 10 W m^{-2} in the peak of summer. The autocorrelation function of the normalized residuals shows some oscillations on top of the decay (Fig. S1). An autoregressive model of order 2 is therefore deemed more appropriate to simulate the normalized residuals.

c. Statistical methods

To properly simulate the weather noise residuals as stochastic noise to be added to the climatology and trend, the statistical properties of the normalized residuals and any links between the forcing variables have to be captured. For example, cloudy low pressure systems can be expected to reduce shortwave radiation while increasing longwave radiation due to the moisture content. Thus, weather-band variability for these two variables is not independent.

Let us thus consider the forcing $\mathbf{X}$ to be multivariate, specifically a $n \times 1$ vector, with n representing the number of forcing variables. We model the state of $\mathbf{X}$ at time t as depending on its previous state, while still incorporating some randomness. This can be represented by an autoregressive process of order p [AR(p)]:

$$\mathbf{X}_t = \sum_{i=1}^{p} \mathbf{\Phi}_i \mathbf{X}_{t-i} + \mathbf{W}_t, \tag{10}$$

where $\mathbf{\Phi}_i$ is an $n \times n$ matrix containing the AR model parameters and $\mathbf{W}$ is a multivariate Gaussian white noise process with mean zero and covariance matrix $\mathbf{\Sigma}_W$. We assume the off-diagonal elements of $\mathbf{\Phi}_i$ to be zero, so that the state of a variable at time t depends only on its own previous state. The model parameters $\mathbf{\Phi}_i$ can be estimated using the autocorrelation function of the previously mentioned normalized residuals (Yule 1927; Walker 1931).

Using a multivariate AR(1) process to model our three ($n = 3$) coupled forcing terms (normalized residuals of longwave radiation, atmospheric temperature, and shortwave radiation), this becomes

$$\mathbf{X}_t = \begin{bmatrix} F_{\mathrm{lw}}^{\mathrm{NRes}} \\ F_{T_a}^{\mathrm{NRes}} \\ F_{\mathrm{sw}}^{\mathrm{NRes}} \end{bmatrix}_t = \begin{bmatrix} \varphi_{\mathrm{lw}} & 0 & 0 \\ 0 & \varphi_{T_a} & 0 \\ 0 & 0 & \varphi_{\mathrm{sw}} \end{bmatrix} \begin{bmatrix} F_{\mathrm{lw}}^{\mathrm{NRes}} \\ F_{T_a}^{\mathrm{NRes}} \\ F_{\mathrm{sw}}^{\mathrm{NRes}} \end{bmatrix}_{t-1} + \begin{bmatrix} w_1 \\ w_2 \\ w_3 \end{bmatrix}_t, \tag{11}$$

with the covariance matrix of the noise given by

$$\mathbf{\Sigma}_W = \sigma_W^2 \begin{bmatrix} 1 & \rho_{12} & \rho_{13} \\ \rho_{21} & 1 & \rho_{23} \\ \rho_{31} & \rho_{32} & 1 \end{bmatrix}, \tag{12}$$

where σ_W is the standard deviation of the noise, $\rho_{12} = \rho_{21}$ is the cross correlation between $F_{\mathrm{lw}}^{\mathrm{NRes}}$ and $F_{T_a}^{\mathrm{NRes}}$, and so on. Covariance between the three forcing variables arises through correlations in the noise forcing $\mathbf{W}_t$ and not through the parameter matrix $\mathbf{\Phi}$. The normalized residuals for the ice–ocean heat flux are generated using an AR(2) model resulting in two parameters $\varphi_{F_w}^1$ and $\varphi_{F_w}^2$ and are assumed to be independent from the surface forcing. The values for all the fitted AR parameters and the cross correlations can be found in Table 1.

Once the normalized residuals have been generated for all forcing variables, they can be scaled by multiplying them by the previously calculated seasonally varying standard deviations σ_{lw}, σ_{T_a}, σ_{sw}, and σ_{F_w}, then added to the climatology (or multiplied in the case of shortwave radiation). The resulting stochastically generated forcing variables can be used to force the model and to investigate the impact of changing variability by modifying the AR parameters φ or scaling the standard deviations σ. If φ's are positive (as is the case here, Table 1), the AR process acts as a low-pass filter of the white noise w and therefore yields a red noise process, with power spectral density decreasing with frequency.

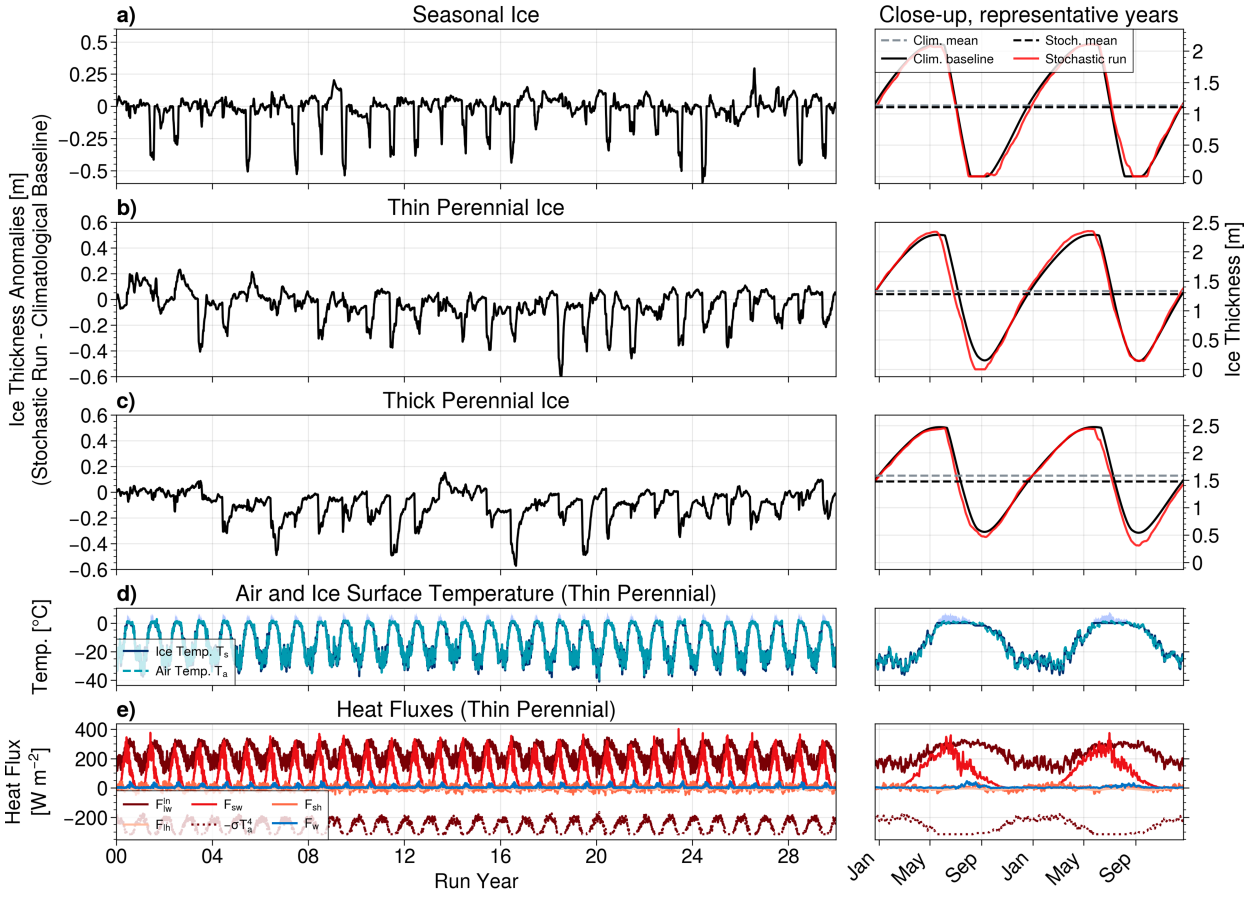

FIG. 3. Typical model run. (left) Difference in ice thickness due to the introduction of zero-mean stochastic noise in the model for the (a) seasonal, (b) thin perennial, and (c) thick perennial ice states. (right) An illustration of the seasonal cycle in two arbitrarily chosen years, for the climatological baseline (black solid line) and the stochastic run (red solid line); and (left) the difference between both lines for the whole model run; the time series means are also provided (excluding first 4 years; dashed lines). The forcing for the thin perennial case is also provided: (d) Atmospheric temperature T_a is provided as input (light blue) and simulated surface ice temperature T_s (dark blue); the light-shaded area indicates the excess heat used to melt ice. (e) Heat fluxes are provided as input, including the climatological latent heat flux.

3. Results

The model is run with three different climatological baselines, representative of different ice states and latitudes: a seasonal ice cover (72°N), a thin perennial ice (75°N), and a thick perennial ice (85°N). The choice of two perennial ice states is motivated by the nonlinearities of the system since we expect the response of the model to depend on its mean state (Massonnet et al. 2018). The model parameter values were chosen to match other studies, after sensitivity experiments provided similar results to the existing scientific literature (see section S2 in the online supplemental material). The simulated ice thickness for each of the climatological baselines is realistic, with the ice varying between 0.0 and 2.1 m for the seasonal ice cover (Fig. 3a, right panel), from 0.3 to 2.3 m in the thin perennial ice (Fig. 3b) and from 0.6 to 2.5 m in the thick perennial ice conditions (Fig. 3c). Two interesting main features can already be observed when comparing the runs with stochasticity (red lines) to the climatological baselines (black lines): 1) the ice thickness anomalies (calculated as the difference between both simulations) exhibit some slow, interannual variability, with a time scale of the order of 7–10 years, and 2) the ice thickness anomalies are nearly always negative, especially for its minimum in the perennial states. These features are investigated in detail in section 3a. The ice surface temperature (Fig. 3d for thin perennial case) follows closely the atmospheric temperature. In summer, the solving of the surface heat balance can lead to a nonphysical ice surface temperature exceeding the melting point (Fig. 3d, light shaded area). The associated excess heat is converted into melting latent heat in the model; the latter internally caps the surface temperature to the melting point.

a. *Sensitivity to forcing noise*

The model is used to investigate the impact of short timescale stochastic forcing on ice thickness mean state and variability. The magnitude of the forcing is scaled by a factor ranging from 0 to 1.5 and then multiplied by the (seasonally varying) standard deviation of each forcing variable. The resulting noise

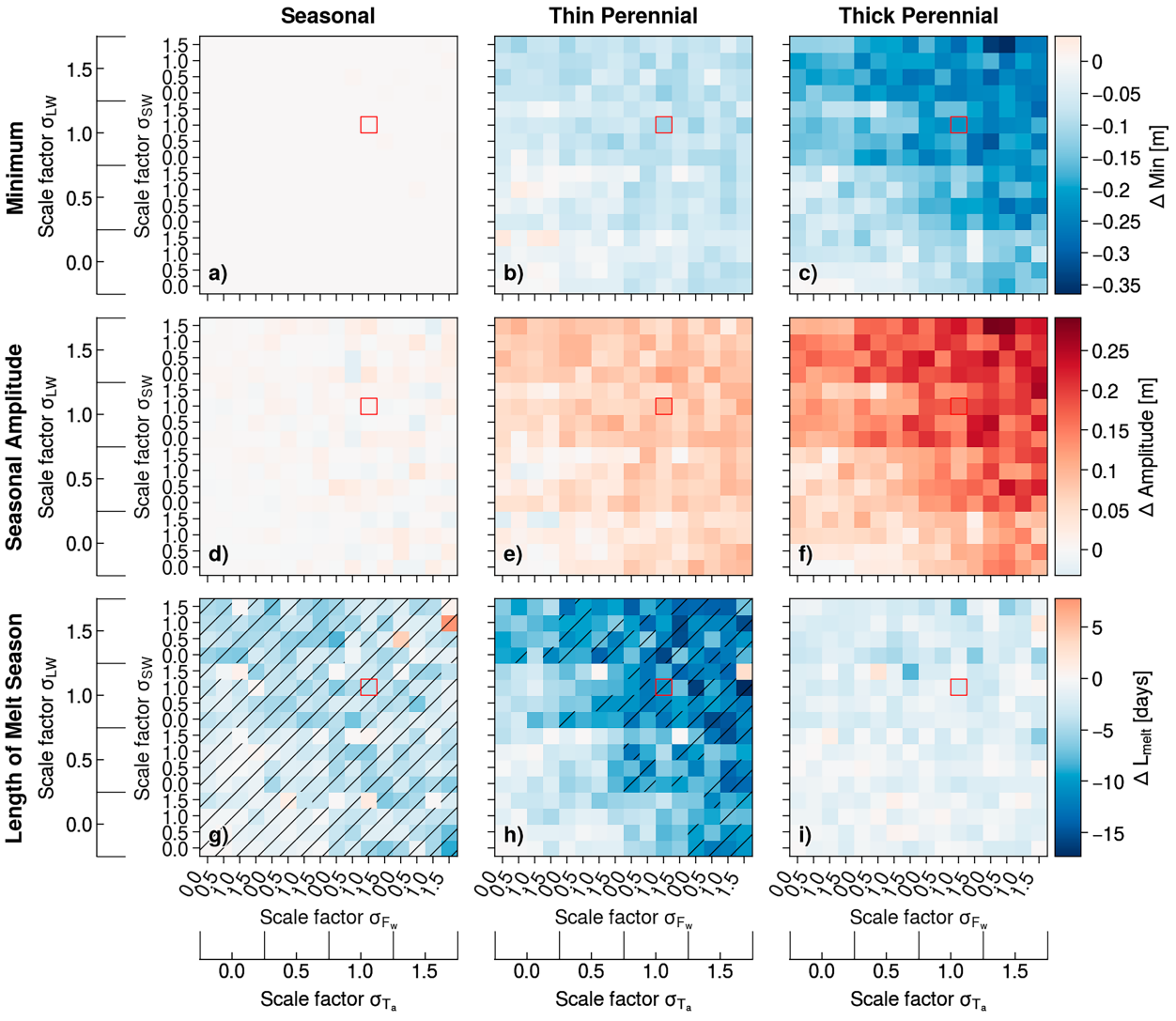

FIG. 4. Nonlinear response of sea ice to stochastic noise. Metrics of ice thickness relative to the climatological baseline (without stochastic noise) for (left) seasonal, (center) thin perennial, and (right) thick perennial sea ice states. (top) Minimum ice thickness, (middle) seasonal amplitude, and (bottom) length of the melt season are calculated for each year of the run after removal of the first 4 spinup years. The metrics from the climatological baseline are then subtracted to obtain anomalies and are finally averaged over the 36 years of the run. The scaling of the variance from 0.0 to 1.5 with 0.5 increments is on the x axis for ice–ocean heat flux F_w (repeated every four grid cells) and for atmospheric temperature T_a (each increment includes four runs; for F_w) and on the y axis for shortwave radiation F_{sw} (repeated every four grid cells) and for longwave radiation F_{lw} (each increment includes four runs; for F_{sw}). Red squares indicate the run with all variance scaling equal to 1. Hashed grid cells indicate runs for which more than half of the years are ice-free in summer.

has a nonstationary (seasonal) variance, but its mean is still zero. It is then added to the climatology to partially reconstruct realistic meteorological and oceanographic conditions at the selected locations. A range of metrics is calculated, including mean ice thickness, amplitude of the seasonal cycle, the day of year of melt onset (identified as the date at which ice thickness reaches its maximum value), and the length of the melting season (calculated as the number of days between the maximum and the minimum ice thicknesses). We run the model for 40 years and discard the first 4 years as spinup, as this is the time necessary for the seasonal cycle to reach a steady state. We then extract the metrics of interest for each of the remaining 36 years. We calculate anomalies by subtracting the metrics of the climatological baseline (no stochastic noise) and average them across all years.

The most striking feature found is the decrease in ice thickness when any zero-mean noise is added, in particular to longwave radiation and atmospheric temperature, for perennial ice states (Figs. 4b,c; see also Fig. 3). The change in the mean ice thickness is driven by a lower ice minimum, while the maximum shows little or no change, resulting in an increased amplitude of the seasonal cycle. The stochastic noise leads to a stronger ice melt and a lower minimum, while the ice growth–thickness feedback brings the thickness maximum back to its climatological

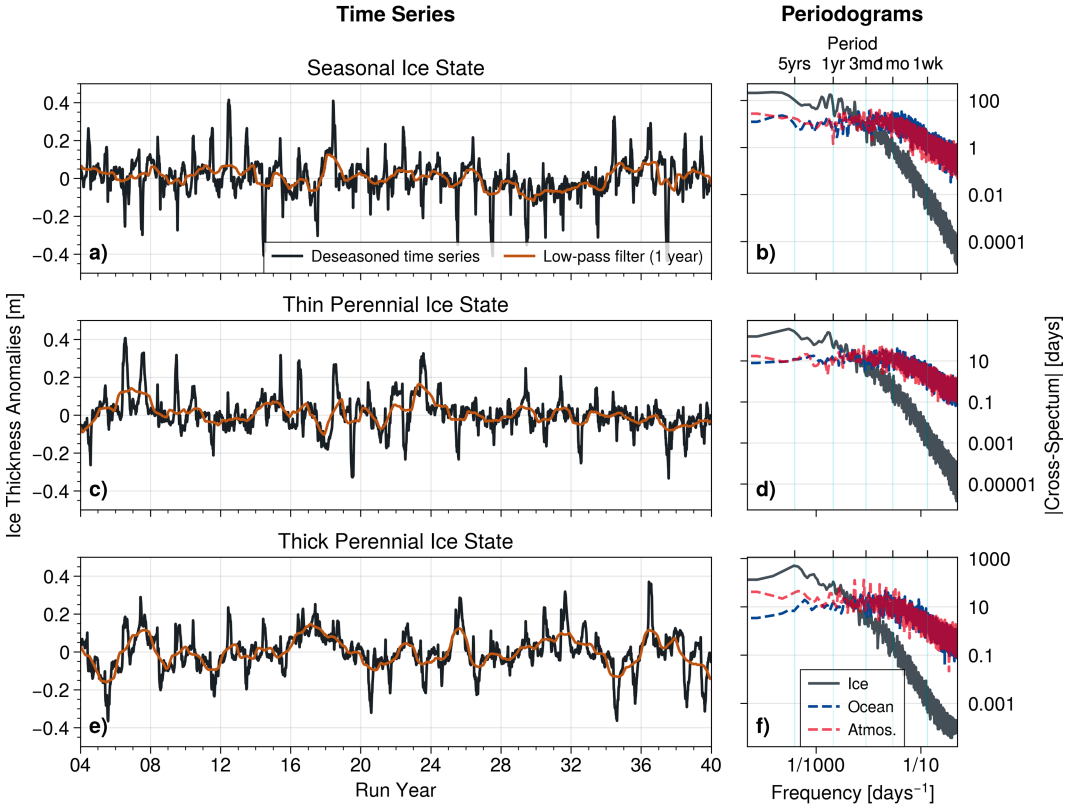

FIG. 5. Deseasonalized ice thickness variability. Modeled ice thickness, once the climatology has been removed, for (a) seasonal, (c) thin perennial, and (e) thick perennial ice states. Here, the climatology is not the same as the climatological baseline: We compute the climatology for the run itself by removing the first 4 spinup years and then using the same climatology calculation as for the ice–ocean heat flux (section 2b). A low-pass filter using a 1-yr bandwidth is also shown (orange line). Periodograms of the deseasonalized, normalized ice thickness (gray), oceanic (blue), and atmospheric forcing (red) are also shown for (b) seasonal, (d) thin perennial, and (f) thick perennial ice states.

baseline, except in the case of thick perennial ice where the thickness remains below the climatological baseline (Fig. 3c). The change in the minimum is of the order of 0.3 m for thick perennial ice, around 40% of its climatological minimum. In the case of thin perennial ice, the stochastic forcing is enough to lead to summer ice-free conditions in most years, shortening the melt season by 15 days (the timing of the maximum is not significantly changed; not shown). In the seasonal ice state, there is no significant difference apart from the added noise. The response of the model is therefore nonlinear: a zero-mean noise leads to a change in the mean state of the ice. It is noteworthy that in all ice states, the impact of the scaling of the noise is mostly linear: more variance means more departure from the climatological mean.

Another feature evident when looking at the time series of the stochastically forced model, using the default standard deviation (scaling of 1.0, i.e., representative of realistic forcing variability), is the emergence of a slow, interannual variability, with a periodicity of 7–10 years, particularly notable when removing the climatology for each individual run (Fig. 5). The model integration of the rapidly fluctuating surface and bottom heat fluxes leads to a strong internal variability. This is in line with the theory of stochastic climate models which integrate the white weather noise into a red oceanic noise response, concentrating the variance at the lower frequencies (Frankignoul and Hasselmann 1977). While the seasonal ice state resets every summer, exhibiting limited interannual variability (Fig. 5a), the perennial ice states allow for year-to-year memory (Figs. 5c,e).

To investigate the frequency domain response of the ice model to the stochastic forcing, periodograms are estimated for the stationary model output, after removing the climatology and normalizing the anomalies. The power spectrum is then computed (Figs. 5b,d,f). The decay of power with increasing frequency confirms the abovementioned integration of the rapid fluctuations of the atmospheric and oceanic noises (red and blue spectra) into a slowly varying red noise and is reminiscent of the stochastic climate models (e.g., Kilpatrick et al. 2011, their Fig. 8). Contrary to the assumed white weather noise used in Hasselmann (1976), our ERA5-based atmospheric and oceanic spectra are flat (white noise) for periods longer than 1 month but are red noise with a small slope for higher frequencies. The cutoff from white to red noise for ice thickness is around the annual period and is less clear since the spectrum still exhibits features for lower frequencies. The peaks in the perennial states at frequencies lower than 1 yr^{-1} confirm the

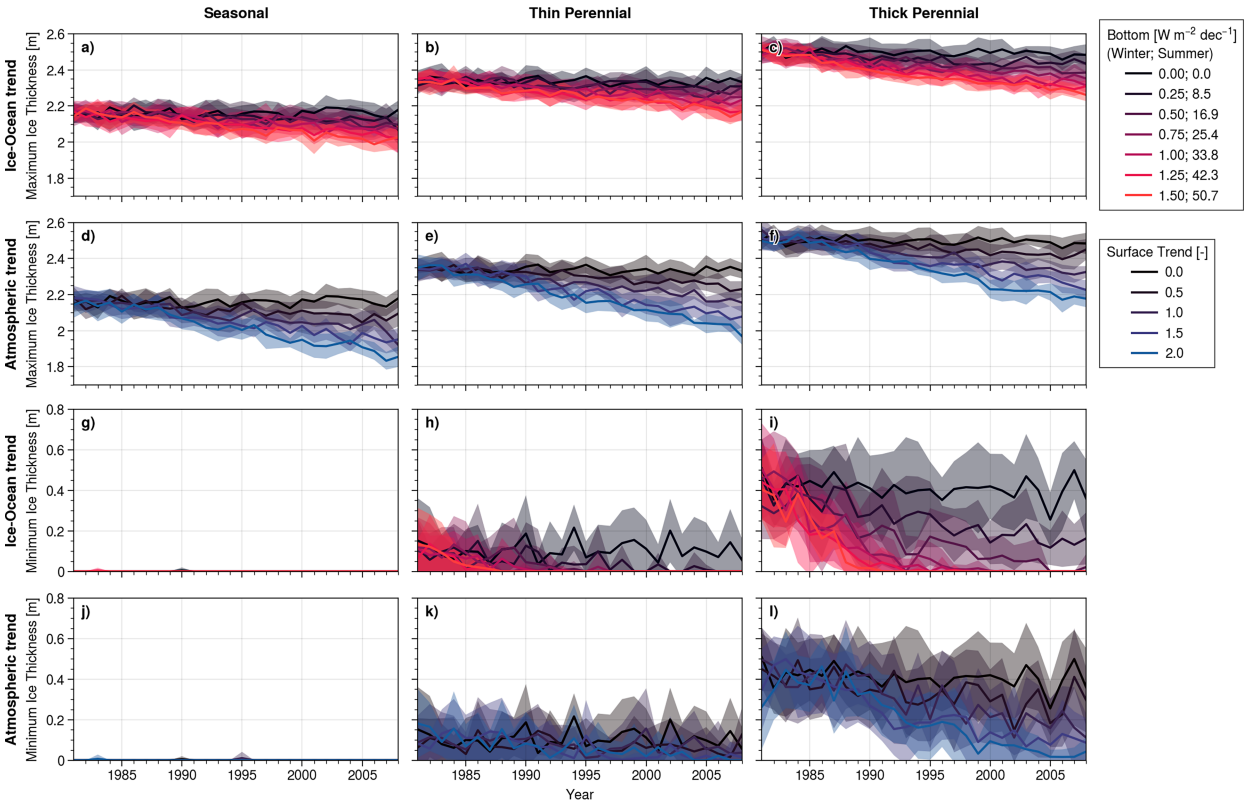

FIG. 6. Impact of forcing trends on ice thickness metrics, for model ensemble run using 30 members (line: ensemble mean; shade: one standard deviation). Impact on annual maximum ice thickness from increasing trend in (a)–(c) ice–ocean heat flux and (d)–(f) atmospheric forcings. (g)–(l) As in (a)–(c) and (d)–(f), but for annual minimum ice thickness. For the bottom trend, the minimum (winter) and maximum (summer) values are provided in the legend.

presence of the interannual variability, though the normalization tends to obscure this. The exact locations of those peaks depend on the realization of the stochastic forcing and therefore on the model run (not shown). Those results are supported by the analysis of a gain function (Fig. S6). A derivation of the model adjustment time scales similar to Thorndike (1992) shows that ice thickness has a quadratic impact on the response time of ice to atmospheric changes (see also SI, section S3). For perennial ice, the memory of the system ranges from months to several years, highlighting how the system can generate low-frequency interannual-to-decadal variability.

b. *Sensitivity to forcing trends*

We have shown that increased variability of the heat fluxes can have impacts on the mean ice thickness. A better understanding of the impact of heat flux trends, both atmospheric and oceanic, is also important to frame the previous results.

We add linear trends of varying magnitudes to the stochastic forcing and run an ensemble of simulations to average out stochastic noise-dependent results (Fig. 6). For the atmospheric forcing, we use the trends extracted from the ERA5 data over the 1979–2021 period (Figs. 2d–f) and scale those trends by a factor between 0.0 (no trend) and 2.0 (twice the ERA5-calculated trend). For the oceanic heat flux trend, we expect a trend stronger in summer than in winter (see section 1) and therefore scale the trend by the seasonal cycle of the ice–ocean heat flux. We use a range of values centered around the winter trend reported by Zhong et al. (2022) (a 0.9 W m^{-2} increase over a 12-yr period), ranging from 0.25 W m^{-2} decade^{-1} (resulting in a summer peak value of 8.5 W m^{-2} decade^{-1}) to 1.5 W m^{-2} decade^{-1} (summer peak value of 50.7 W m^{-2} decade^{-1}). The model is first run 4 years without trend for spinup, then run for 26 years with trends.

Unsurprisingly, the trends lead to a decrease in maximum and minimum ice thickness, except in the seasonal ice state where the minimum is already at zero (Fig. 6). The slope of the ice thickness anomaly decreases in magnitude with time, leading to a deceleration of ice thinning, despite the linearly increasing trend in the forcing. This is most apparent for the maximum ice thickness in the thick perennial state (Fig. 6c) and can be explained by the ice growth–thickness feedback: a thinner ice can recover faster during the freezing season. This is yet another consequence of the nonlinearities of the system. Another feature is the stronger impact of the ice–ocean heat flux trend compared to the atmospheric trends for the minimum thickness (Figs. 6g–i). Both perennial ice states turn to seasonal ones within 20 years when applying an ice–ocean heat flux trend, except for the smallest trend (Figs. 6h,i). In particular, even for the thick perennial ice state, winter trends equal to or above 0.75 W m^{-2} decade^{-1} (25.4 W m^{-2} decade^{-1} at the

peak of summer) lead to ice-free summers for all members of the ensembles (shaded areas indicate the ensemble standard deviation). For the maximum ice thickness, the atmospheric heat flux seems to have more impact than the ice–ocean heat flux. This can be understood when looking at the actual slopes of the atmospheric trends which are overall positive in winter (during the ice growing season) but close to zero or even negative for the shortwave radiation in summer (Figs. 2d–f). It therefore makes sense that the ice–ocean heat flux drives the summer minimum ice thickness, while the atmospheric trend dominates the winter maximum thickness. The impacts of trends are also stronger for the ice minimum than for the maximum. For example, a realistic atmospheric trend (factor of 1.0) leads to an ensemble mean decrease over the 30 years of 0.1 m for the maximum thickness, and a loss of 0.2 m for the minimum thickness, in the thick perennial state. The ice–ocean heat flux trends also lead to a stronger response of the minimum thickness compared to the maximum, with a loss of 0.5 m in the minimum, compared to 0.15 m for the maximum. Note that the ensemble spread is also higher for the minimum. While the ice system is nonlinear as demonstrated throughout the study, the superposition of both trends still leads to a mostly linear superposition of the results. Oceanic trends have a stronger impact on minimum ice thickness and a stronger influence on when ice-free summers will happen, while atmospheric trends have a slightly stronger impact on maximum ice thickness decline (Fig. S7).

4. Discussion

We have used a zero-layer ice thickness model to investigate the response of sea ice thickness to stochastic heat flux forcing. This model is quite simple: it balances heat fluxes at the atmosphere–ice and ocean–ice interfaces through vertical heat diffusion to estimate ice growth and melt at the surface and bottom. It captures the albedo positive feedback and the ice growth–thickness feedback, two of the most important processes that control ice melt and growth. The real strength of such a simple model is its direct link between processes, results, and interpretation. This allows for a robust process-oriented understanding of the behavior of the model, despite the relative complexity of the nonlinear processes involved. Another significant advantage is the relatively low computational cost of the model, allowing for model ensemble simulations over decades, necessary for the stochastic context used here.

Nonetheless, the predictive skill of the model remains an important question, as a number of simplifications are used: the model assumes no heat capacity (the temperature gradient within the ice is linear), no brine pockets or channels potentially altering the conductivity or the latent heat vertically or temporally (Vancoppenolle et al. 2009; Worster and Rees Jones 2015), no snow layer insulating the ice (although the formulation accounts for the snow albedo), no penetration of solar radiation, and no dynamics or rheology of the ice (e.g., Hibler 1979). We focus here on qualitative behavior and restrain from quantitatively validating the model, though initial studies using the zero-layer model have shown a good agreement with more complex thermodynamical ice models (Semtner 1976). As in those earlier studies, our model does not account for rheology nor ice dynamics. This is deemed acceptable in most cases, as sea ice dynamics explain at most 20% of sea ice loss (Le Guern-Lepage and Tremblay 2023). In regions where dynamics are relevant, such as Fram Strait and the East Greenland Current, caution should be used when applying our results, not only because the dynamics are not included in our model but also because thermodynamics might be significantly affected. For example, advection of ice toward warmer waters could induce an oceanic heat flux variability outside the range explored in this study. Nonetheless, sea ice is primarily controlled by thermodynamics, through its high albedo and insulation properties. We account for both, albeit in a simple form. The model results are not strongly sensitive to a more complex formulation of the albedo parameterization (not shown), i.e., one which includes a temperature threshold below the melting point at which albedo begins to decrease (e.g., Lindsay and Rothrock 1993) and a linear change in albedo above this threshold. Sea ice is a complex, multiphase medium, whose thermal properties vary spatially and temporally, but simpler models that do not incorporate those variations, such as the one used here, still show an overall good agreement with observations (e.g., Maykut and Untersteiner 1971; Semtner 1976; Thorndike 1992). The use of a single ice layer is also at odds with the typical multilayer models used in many of the most recent ice models. Yet, the model results are not strongly sensitive to internal heat capacity in the ice, which we represented by the addition of an extra ice layer. The rectifying effect (Fig. S8) and the internal variability generation (not shown) are still clearly visible in the results from the model with internal heat capacity. Interestingly, the rectifying effect is slightly more pronounced in this model (Fig. S8). This is due to the introduction of a piecewise linear temperature profile, resulting in an overall less variable conductive ice flux within the ice, leading to a stronger integration of the fast weather fluctuations into the mean state. The introduction of a snow layer would likely result in a stronger though similar effect due to the lower thermal conductivity of snow. The results presented in this study, based on the zero-layer model, are therefore likely conservative, and stronger nonlinear behavior is to be expected for more complex models. Finally, by comparing general circulation models from the CMIP5 ensemble and including their own version of a Semtner (1976) zero-layer model, Massonnet et al. (2018) found that the complexity of ice models is not correlated with their skill in simulating mean ice state, freezing, and melting. We are therefore confident that this zero-layer simple ice model is fit for the purpose for our study objectives.

As mentioned in the introduction, other studies have used simple models to investigate the stability of the ice system (Wagner and Eisenman 2015; Moon and Wettlaufer 2011, 2013, 2017). Those studies are based on a one-column, enthalpy-based sea ice–mixed layer model aimed at representing conditions at the scale of the whole Arctic region (Eisenman and Wettlaufer 2009); our model differs fundamentally from their approach by representing ice conditions over a much smaller spatial scale and focusing on the response of sea ice thickness and surface temperature to local meteorological and oceanic fluctuations. We do not parameterize ice import or export in our model. Compared to the Eisenman and Wettlaufer (2009)

formulation, our model includes some simplifications, such as a simpler albedo formulation and a lack of shortwave penetration into the ice. However, our model also includes more complex treatment of some processes, including a bottom temperature at the freezing point instead of the melting point (meaning the heat conductive flux in the ice can change sign depending on the surface temperature), and more importantly, a realistically time-varying ice–ocean heat flux instead of a constant one. Moreover, this study introduces an important novelty in the treatment of statistical noise representation. Some mathematical studies have investigated the influence of noise (e.g., Moon and Wettlaufer 2013, 2017), either additive or multiplicative in form, but without formulating the noise based on known observational forms. From a mathematical perspective, their central focus is to turn their continuous time formulation of a stochastic model into a discrete system, which can affect the numerical scheme. Our approach is based on a discretized (in time) form of the continuous deterministic ordinary differential (5). We then inject discrete time stochasticity via multivariate autoregressive models, interpolated on the model time step. From a physical perspective, the studies by Moon and Wettlaufer (2013, 2017) mainly focus on distinguishing between pan-Arctic stable ice states (ice-free, seasonal, or perennial ice cover) and the switch between them in response to an external heat flux mimicking greenhouse gas forcing. In opposition, our noise and trends for both atmospheric and oceanic forcing are formulated based on well-calibrated observational, model, and reanalysis products and are properly scaled to best match the realistic evolution of local forcing. Our emphasis is on the response of the nonlinear ice system to those realistic noises and trends, independent of a state change. We also investigate the sensitivity of the system to noise amplitudes and include not only a seasonally varying oceanic forcing but also stochastic noise and trends for this forcing, contrary to Moon and Wettlaufer (2017). It is worth noting that the rectification process highlighted in this study confirms and expands on the existence of a "memory effect," investigated by Moon and Wettlaufer (2017) for the divergence between ice states at the end of summer.

The ice thickness exhibits a nonlinear response to stochastic forcing, wherein a zero-mean stochastic noise added onto the climatological forcing generates a nonzero response in the mean thickness state (Fig. 7b). The conditional form of (5) can explain this surprising response (Fig. 7a), as increased variability can drive ice surface temperature to reach the melting point sooner than under climatological conditions, triggering the albedo feedback process to melt more ice. Hence, sea ice acts as a rectifier. The nonlinear formulation of the outgoing longwave radiation, varying to the fourth power of the surface temperature, would also emphasize positive anomalies over negative anomalies, leading to a net negative ice thickness anomaly. But the induced outgoing longwave anomaly would be 1–2 orders of magnitude lower than the baseline, and therefore negligible. The ice growth–thickness feedback can partially compensate for this ice loss if the ice gets thin enough. While the quantitative aspect of this result is a consequence of the formulation and parameters used, it has physical grounds since snow and ice change their albedo significantly once they start to melt or to turn to slush. The albedo feedback is a well-understood and validated process. This mean state offset has implications for model validation and simulations: a model run under climatological forcing should not be quantitatively validated against observations, as noise needs to be accounted for to generate realistic mean statistics. Similarly, using spatially averaged forcing will smooth the noisiness of the forcing variable and therefore lead to a mean bias in the ice thickness. This could be a potential factor in the underestimation of ice sensitivity and decline in Earth system models (Stroeve et al. 2007; Rampal et al. 2011; Notz and SIMIP Community2020).

The impact of the high-frequency forcing variability is also visible in the frequency domain, as the periodogram exhibits a decreasing slope at high frequencies. This hints at an inverse energy cascade, as the energy input at short time scales is transferred to longer time scales (Fig. 7b). The transfer of energy across time scales through harmonic generation arises from nonlinearities in the equations including, famously, in turbulence theory (Richardson 1922; Bailly and Comte-Bellot 2015). Nonlinear terms are also evident in the equations governing the evolution of sea ice thickness [(5)]. Here, we draw an analogy between the nonlinear transfer of energy toward low frequency by sea ice and other physical processes such as the generation of harmonics in internal waves by reflection at a pycnocline (Thorpe 1998) or in surface currents by wind friction (Militello and Kraus 2001). The inverse energy cascade unveiled here highlights the role of sea ice as a climate component, dampening the variability on daily to weekly time scale to generate seasonal-to-interannual variability. As mentioned in the introduction, stochastic climate models have been a fruitful approach to explain the generation of such low-frequency internal variability in the climate system. This study builds on those earlier works and extends the results to a cyclostationary system, with a seasonal cycle taken into account (as in Moon and Wettlaufer 2017). This is a step forward, as the conceptual models used by Hasselmann (1976) and Frankignoul and Hasselmann (1977) only focus on anomalies around the seasonal cycle.

The rapid climate changes occurring in the Arctic have consequences for the variability of the heat fluxes. A shift in the storm track location or the increased generation of clouds leads to a decrease in shortwave radiation in summer and an increase in longwave radiation, especially in winter and during the shoulder seasons. In light of the response of the ice to increased variability of longwave radiation, we can expect a negative anomaly in ice thickness, leading to thinner ice and increased seasonal amplitude in perennial ice regions (Fig. 7c). This feature is independent of the trend. The positive trends of longwave radiation and atmospheric temperature, mostly occurring in winter and in the shoulder seasons, go together with a negative trend of solar radiation in summer. This results in an overall negative trend of ice thickness, especially for the maximum, along with increased variance in the timing of the melt onset and the minimum value. Note that since the trend used here is derived for the period covering 1979–2021, it is likely a conservative estimate of the trend for more recent years and for the next decades. We can therefore expect the trend for ice thickness to be on the order of -0.1 m decade^{-1} or lower (corresponding to a slope factor in the atmospheric trends of 1.5 or 2) rather than around -0.05 m decade^{-1} (slope factor of 1.0). On top of this temporal aspect,

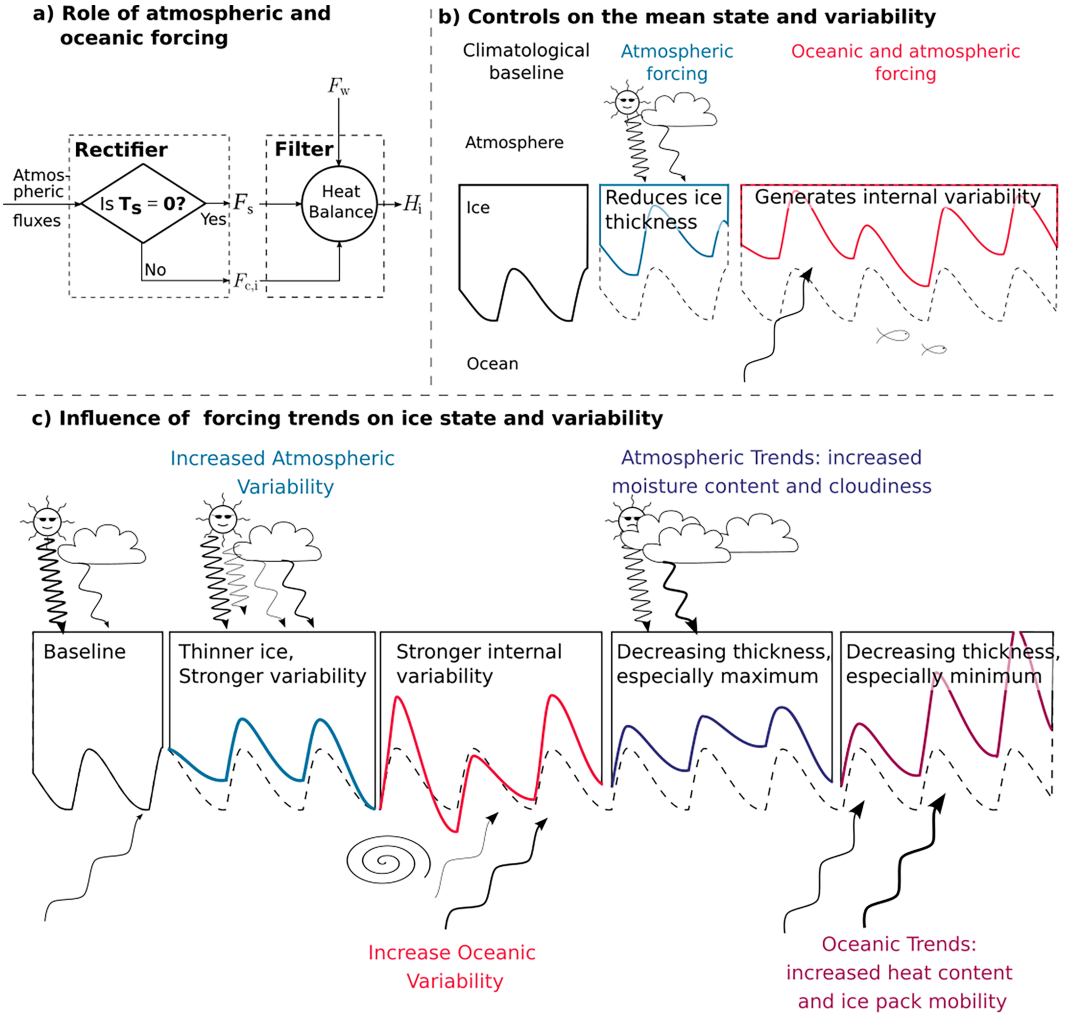

FIG. 7. Conceptual summary of the results. (a) Ice model seen as the combination of a rectifier of atmospheric fluxes and a low-pass filter for ice–ocean, atmospheric, and conductive heat fluxes [(5)]. (b) Impacts of stochastic noise in forcing on ice thickness: atmospheric noise reduces ice thickness, while both atmospheric and oceanic noises generate internal variability. (c) Projected changes in ice thickness due to anthropogenic climate change: increased atmospheric variability due to changes in storm tracks or cloud nucleation leads to thinner ice, while increased eddy variability of the Arctic Ocean leads to stronger internal variability. Increased winter longwave radiation and decreased summer shortwave radiation due to increased moisture content and cloudiness lead to decreasing ice thickness, especially in winter, while increased oceanic heat content and ice pack mobility strongly decrease ice thickness, especially in summer.

there is also some spatial variability in the expected trends. For example, the North Pacific storm track is expected to shift poleward, leading to more cyclones over the Beaufort Gyre (Crawford and Serreze 2017). This would enhance the heat flux variability and lead to a negative anomaly for ice thickness over the Canadian side of the Arctic.

Yet, according to our results, the trend in atmospheric forcing is less important in setting the future of sea ice than the trends in the ice–ocean heat flux, in line with Merryfield et al. (2008). While the positive trend for the atmospheric forcing variables is mostly occurring in winter or in the shoulder seasons, and is even slightly negative in summer for the shortwave radiation, the positive trend for the ice–ocean heat flux is expected to accelerate in summer, through a longer open water season leading to higher mixed-layer temperature and a more mobile ice pack leading to stronger sensible heat flux (Fig. 7c). This is likely to be the dominant driver for the decline in sea ice in summer. Just as for atmosphere–ice heat fluxes, some spatial variability can be expected for the ice–ocean heat flux trends, with a stronger increase near the Arctic gateways (Fram and Bering Straits and Barents Sea Opening; see Rudels 2015 for locations). A significant limitation of this result is the lack of robust estimates on the past, current, and future trends of the ice–ocean heat flux, including its seasonality. We carefully built our parameterization, but none of the sources used are independently able to realistically constrain the ice–ocean

heat flux. Nonetheless, we consider our parameterization as encompassing the likely trend in a conservative way, as summer-averaged ice–ocean heat fluxes above 100 W m^{-2} are thought to have explained some of the recent multiyear ice losses (MacKinnon et al. 2021; Babb et al. 2022). Increased variability of the ice–ocean heat flux does not generate a significant response in the mean ice state, so the increased frequency of eddies in the Arctic Ocean (Von Appen et al. 2022) should not produce an offset similar to increased longwave radiation or atmospheric temperature in the ice mean state. But the increased energy at high frequencies is still expected to yield increased low-frequency variability. This could lead to less predictable sea ice at seasonal-to-interannual time scales in perennial ice conditions, until reaching a seasonal state where the memory resets. A concerted effort for observationally constraining ice–ocean heat flux seasonality, variability, and trend would provide critical information to better understand and predict the fate of sea ice and the redistribution of energy at the different time scales of the weather–climate systems.

This study provides a picture of sea ice as an integral component of the climate system, absorbing high-frequency variability into its mean state as well as cascading energy from weather noise to climate variability. The fate of sea ice as a seasonal rather than perennial system would reduce its capacity to integrate variability at interannual time scales, as the absence of ice in summer would reset its "memory." This could have significant consequences on the atmospheric and the oceanic systems, considering how tightly it is intertwined with those climate components.

Acknowledgments. This work is supported by the National Sciences and Engineering Research Council of Canada Discovery Grant RGPIN-2018-05255, the Ocean Frontier Institute through an award from the Canada First Research Excellence Fund, and ArcticNet, a Network of Centres of Excellence Canada. The authors wish to express their gratitude to the editor Dr. Shawn Marshall and three anonymous reviewers for their constructive comments and recommendations.

Data availability statement. The model is publicly available at https://github.com/bnjmnr/SimpleIceModel_Semtner76. The ERA5 reanalysis data (Hersbach et al. 2020) were downloaded from the Copernicus Climate Change Service (C3S). The ice-tethered profiler data were collected and made available by the Ice-Tethered Profiler Program (Toole et al. 2011; Krishfield et al. 2008) based at the Woods Hole Oceanographic Institution.

REFERENCES

Ardyna, M., and K. R. Arrigo, 2020: Phytoplankton dynamics in a changing Arctic Ocean. *Nat. Climate Change*, **10**, 892–903, https://doi.org/10.1038/s41558-020-0905-y.

Arrigo, K. R., and G. L. van Dijken, 2011: Secular trends in Arctic Ocean net primary production. *J. Geophys. Res.*, **116**, C09011, https://doi.org/10.1029/2011JC007151.

Babb, D. G., R. J. Galley, S. E. L. Howell, J. C. Landy, J. C. Stroeve, and D. G. Barber, 2022: Increasing multiyear sea ice loss in the Beaufort Sea: A new export pathway for the diminishing multiyear ice cover of the Arctic Ocean. *Geophys. Res. Lett.*, **49**, e2021GL097595, https://doi.org/10.1029/2021GL097595.

Bailly, C., and G. Comte-Bellot, 2015: Introduction to turbulence. *Turbulence*, C. Bailly and G. Comte-Bellot, Eds., Experimental Fluid Mechanics, Springer, 1–31, https://doi.org/10.1007/978-3-319-16160-0_1.

Bitz, C. M., and G. H. Roe, 2004: A mechanism for the high rate of sea ice thinning in the Arctic Ocean. *J. Climate*, **17**, 3623–3632, https://doi.org/10.1175/1520-0442(2004)017<3623:AMFTHR>2.0.CO;2.

Boetius, A., and Coauthors, 2013: Export of algal biomass from the melting Arctic sea ice. *Science*, **339**, 1430–1432, https://doi.org/10.1126/science.1231346.

Crawford, A. D., and M. C. Serreze, 2017: Projected changes in the arctic frontal zone and summer arctic cyclone activity in the CESM large ensemble. *J. Climate*, **30**, 9847–9869, https://doi.org/10.1175/JCLI-D-17-0296.1.

Cunsolo Willox, A., S. L. Harper, V. L. Edge, K. Landman, K. Houle, and J. D. Ford, 2013a: The land enriches the soul: On climatic and environmental change, affect, and emotional health and well-being in Rigolet, Nunatsiavut, Canada. *Emotion Space Soc.*, **6**, 14–24, https://doi.org/10.1016/j.emospa.2011.08.005.

——, ——, J. D. Ford, V. L. Edge, K. Landman, K. Houle, S. Blake, and C. Wolfrey, 2013b: Climate change and mental health: An exploratory case study from Rigolet, Nunatsiavut, Canada. *Climatic Change*, **121**, 255–270, https://doi.org/10.1007/s10584-013-0875-4.

DeGrandpre, M., W. Evans, M.-L. Timmermans, R. Krishfield, B. Williams, and M. Steele, 2020: Changes in the Arctic Ocean carbon cycle with diminishing ice cover. *Geophys. Res. Lett.*, **47**, e2020GL088051, https://doi.org/10.1029/2020GL088051.

Di Lorenzo, E., and M. D. Ohman, 2013: A double-integration hypothesis to explain ocean ecosystem response to climate forcing. *Proc. Natl. Acad. Sci. USA*, **110**, 2496–2499, https://doi.org/10.1073/pnas.1218022110.

Ditlevsen, P., and S. Ditlevsen, 2023: Warning of a forthcoming collapse of the Atlantic meridional overturning circulation. *Nat. Commun.*, **14**, 4254, https://doi.org/10.1038/s41467-023-39810-w.

Duke, P. J., and Coauthors, 2023: Canada's marine carbon sink: An early career perspective on the state of research and existing knowledge gaps. *FACETS*, **8**, 1–21, https://doi.org/10.1139/facets-2022-0214.

Eisenman, I., and J. S. Wettlaufer, 2009: Nonlinear threshold behavior during the loss of Arctic sea ice. *Proc. Natl. Acad. Sci. USA*, **106**, 28–32, https://doi.org/10.1073/pnas.0806887106.

Flato, G. M., and R. D. Brown, 1996: Variability and climate sensitivity of landfast Arctic sea ice. *J. Geophys. Res.*, **101**, 25 767–25 777, https://doi.org/10.1029/96JC02431.

Frankignoul, C., and K. Hasselmann, 1977: Stochastic climate models, part II Application to sea-surface temperature anomalies and thermocline variability. *Tellus*, **29**, 289–305, https://doi.org/10.1111/j.2153-3490.1977.tb00740.x.

Goosse, H., 1998: Modelling the large-scale behaviour of the coupled ocean-sea-ice system. Ph.D. thesis, Université Catholique de Louvain, 231 pp.

——, and Coauthors, 2018: Quantifying climate feedbacks in polar regions. *Nat. Commun.*, **9**, 1919, https://doi.org/10.1038/s41467-018-04173-0.

Hasselmann, K., 1976: Stochastic climate models Part I. Theory. *Tellus*, **28**, 473–485, https://doi.org/10.1111/j.2153-3490.1976.tb00696.x.

Hersbach, H., and Coauthors, 2020: The ERA5 global reanalysis. *Quart. J. Roy. Meteor. Soc.*, **146**, 1999–2049, https://doi.org/10.1002/qj.3803.

Hibler, W. D., III, 1979: A dynamic thermodynamic sea ice model. *J. Phys. Oceanogr.*, **9**, 815–846, https://doi.org/10.1175/1520-0485(1979)009<0815:ADTSIM>2.0.CO;2.

Holland, M. M., and E. C. Hunke, 2022: A review of Arctic sea ice climate predictability in large-scale Earth system models. *Oceanography*, **35** (3–4), 20–27, https://doi.org/10.5670/oceanog.2022.113.

——, C. M. Bitz, and B. Tremblay, 2006: Future abrupt reductions in the summer Arctic sea ice. *Geophys. Res. Lett.*, **33**, L23503, https://doi.org/10.1029/2006GL028024.

IPCC, 2021: Annex VII: Glossary. *Climate Change 2021: The Physical Science Basis*, V. Masson-Delmotte et al., Eds., Cambridge University Press, 2215–2256, https://doi.org/10.1017/9781009157896.022.

Kilpatrick, T., N. Schneider, and E. D. Lorenzo, 2011: Generation of low-frequency spiciness variability in the thermocline. *J. Phys. Oceanogr.*, **41**, 365–377, https://doi.org/10.1175/2010JPO4443.1.

Krishfield, R. A., and D. K. Perovich, 2005: Spatial and temporal variability of oceanic heat flux to the Arctic ice pack. *J. Geophys. Res.*, **110**, C07021, https://doi.org/10.1029/2004JC002293.

——, J. Toole, A. Proshutinsky, and M.-L. Timmermans, 2008: Automated ice-tethered profilers for seawater observations under pack ice in all seasons. *J. Atmos. Oceanic Technol.*, **25**, 2091–2105, https://doi.org/10.1175/2008JTECHO587.1.

Lannuzel, D., and Coauthors, 2020: The future of Arctic sea-ice biogeochemistry and ice-associated ecosystems. *Nat. Climate Change*, **10**, 983–992, https://doi.org/10.1038/s41558-020-00940-4.

Le Guern-Lepage, A., and B. L. Tremblay, 2023: Disentangling dynamic from thermodynamic summer ice area loss from observations (1979–2021): A potential mechanism for a "first-time" ice-free Arctic. *J. Climate*, **36**, 7693–7713, https://doi.org/10.1175/JCLI-D-22-0628.1.

Lemke, P., E. W. Trinkl, and K. Hasselmann, 1980: Stochastic dynamic analysis of polar sea ice variability. *J. Phys. Oceanogr.*, **10**, 2100–2120, https://doi.org/10.1175/1520-0485(1980)010<2100:SDAOPS>2.0.CO;2.

Lenton, T. M., H. Held, E. Kriegler, J. W. Hall, W. Lucht, S. Rahmstorf, and H. J. Schellnhuber, 2008: Tipping elements in the Earth's climate system. *Proc. Natl. Acad. Sci. USA*, **105**, 1786–1793, https://doi.org/10.1073/pnas.0705414105.

Light, B., and Coauthors, 2022: Arctic sea ice albedo: Spectral composition, spatial heterogeneity, and temporal evolution observed during the MOSAiC drift. *Elementa*, **10**, 000103, https://doi.org/10.1525/elementa.2021.000103.

Lindsay, R., and D. Rothrock, 1993: The calculation of surface temperature and albedo of Arctic sea ice from AVHRR. *Ann. Glaciol.*, **17**, 391–397, https://doi.org/10.3189/S026030550001315X.

Liu, G., Y.-O. Kwon, C. Frankignoul, and J. Lu, 2023: Understanding the drivers of Atlantic multidecadal variability using a stochastic model hierarchy. *J. Climate*, **36**, 1043–1058, https://doi.org/10.1175/JCLI-D-22-0309.1.

MacKinnon, J. A., and Coauthors, 2021: A warm jet in a cold ocean. *Nat. Commun.*, **12**, 2418, https://doi.org/10.1038/s41467-021-22505-5.

Massonnet, F., M. Vancoppenolle, H. Goosse, D. Docquier, T. Fichefet, and E. Blanchard-Wrigglesworth, 2018: Arctic sea-ice change tied to its mean state through thermodynamic processes. *Nat. Climate Change*, **8**, 599–603, https://doi.org/10.1038/s41558-018-0204-z.

Maykut, G. A., 1986: The surface heat and mass balance. *The Geophysics of Sea Ice*, N. Untersteiner, Ed., Springer, 395–463, https://doi.org/10.1007/978-1-4899-5352-0_6.

——, and N. Untersteiner, 1971: Some results from a time-dependent thermodynamic model of sea ice. *J. Geophys. Res.*, **76**, 1550–1575, https://doi.org/10.1029/JC076i006p01550.

——, and M. G. McPhee, 1995: Solar heating of the Arctic mixed layer. *J. Geophys. Res.*, **100**, 24 691–24 703, https://doi.org/10.1029/95JC02554.

McPhee, M. G., 2008: *Air-Ice-Ocean Interaction: Turbulent Ocean Boundary Layer Exchange Processes*. Springer, 215 pp.

Meehl, G. A., and W. M. Washington, 1990: CO_2 climate sensitivity and snow-sea-ice albedo parameterization in an atmospheric GCM coupled to a mixed-layer ocean model. *Climatic Change*, **16**, 283–306, https://doi.org/10.1007/BF00144505.

Meier, W. N., and J. Stroeve, 2022: An updated assessment of the changing Arctic sea ice cover. *Oceanography*, **35** (3–4), 10–19, https://doi.org/10.5670/oceanog.2022.114.

Merryfield, W. J., M. M. Holland, and A. H. Monahan, 2008: Multiple equilibria and abrupt transitions in Arctic summer sea ice extent. *Arctic Sea Ice Decline: Observations, Projections, Mechanisms, and Implications*, Geophysical Monograph Series, Vol. 180, Amer. Geophys. Union, 151–174, https://doi.org/10.1029/180GM11.

Middleton, J., A. Cunsolo, A. Jones-Bitton, I. Shiwak, M. Wood, N. Pollock, C. Flowers, and S. L. Harper, 2020a: "We're people of the snow:" Weather, climate change, and Inuit mental wellness. *Soc. Sci. Med.*, **262**, 113137, https://doi.org/10.1016/j.socscimed.2020.113137.

——, ——, ——, C. J. Wright, and S. L. Harper, 2020b: Indigenous mental health in a changing climate: A systematic scoping review of the global literature. *Environ. Res. Lett.*, **15**, 053001, https://doi.org/10.1088/1748-9326/ab68a9.

Militello, A., and N. C. Kraus, 2001: Generation of harmonics by sea breeze in nontidal water bodies. *J. Phys. Oceanogr.*, **31**, 1639–1647, https://doi.org/10.1175/1520-0485(2001)031<1639:GOHBSB>2.0.CO;2.

Moon, W., and J. S. Wettlaufer, 2011: A low-order theory of Arctic sea ice stability. *Europhys. Lett.*, **96**, 39001, https://doi.org/10.1209/0295-5075/96/39001.

——, and ——, 2013: A stochastic perturbation theory for non-autonomous systems. *J. Math. Phys.*, **54**, 123303, https://doi.org/10.1063/1.4848776.

——, and ——, 2017: A stochastic dynamical model of Arctic sea ice. *J. Climate*, **30**, 5119–5140, https://doi.org/10.1175/JCLI-D-16-0223.1.

Notz, D., and SIMIP Community, 2020: Arctic sea ice in CMIP6. *Geophys. Res. Lett.*, **47**, e2019GL086749, https://doi.org/10.1029/2019GL086749.

Perovich, D. K., and C. Polashenski, 2012: Albedo evolution of seasonal Arctic sea ice. *Geophys. Res. Lett.*, **39**, L08501, https://doi.org/10.1029/2012GL051432.

Rampal, P., J. Weiss, C. Dubois, and J.-M. Campin, 2011: IPCC climate models do not capture Arctic sea ice drift acceleration: Consequences in terms of projected sea ice thinning and decline. *J. Geophys. Res.*, **116**, C00D07, https://doi.org/10.1029/2011JC007110.

Rantanen, M., A. Y. Karpechko, A. Lipponen, K. Nordling, O. Hyvärinen, K. Ruosteenoja, T. Vihma, and A. Laaksonen, 2022: The Arctic has warmed nearly four times faster than

the globe since 1979. *Commun. Earth Environ.*, **3**, 168, https://doi.org/10.1038/s43247-022-00498-3.

Renkl, C., E. C. J. Oliver, and K. R. Thompson, 2024: Downscaling the ocean response to the Madden-Julian oscillation in the northwest Atlantic and adjacent shelf seas. *Climate Dyn.*, **62**, 6719–6744, https://doi.org/10.1007/s00382-024-07233-y.

Richardson, L. F., 1922: *Weather Prediction by Numerical Process.* Cambridge University Press, 236 pp.

Richaud, B., K. Fennel, E. C. J. Oliver, M. D. DeGrandpre, T. Bourgeois, X. Hu, and Y. Lu, 2023: Underestimation of oceanic carbon uptake in the Arctic Ocean: Ice melt as predictor of the sea ice carbon pump. *Cryosphere*, **17**, 2665–2680, https://doi.org/10.5194/tc-17-2665-2023.

Rudels, B., 2015: Arctic Ocean circulation, processes and water masses: A description of observations and ideas with focus on the period prior to the International Polar Year 2007–2009. *Prog. Oceanogr.*, **132**, 22–67, https://doi.org/10.1016/j.pocean.2013.11.006.

Rysgaard, S., and Coauthors, 2011: Sea ice contribution to the air–sea CO_2 exchange in the Arctic and Southern Oceans. *Tellus*, **63B**, 823–830, https://doi.org/10.1111/j.1600-0889.2011.00571.x.

Semtner, A. J., Jr., 1976: A model for the thermodynamic growth of sea ice in numerical investigations of climate. *J. Phys. Oceanogr.*, **6**, 379–389, https://doi.org/10.1175/1520-0485(1976)006<0379:AMFTTG>2.0.CO;2.

Serreze, M. C., and J. A. Francis, 2006: The Arctic amplification debate. *Climatic Change*, **76**, 241–264, https://doi.org/10.1007/s10584-005-9017-y.

Spreen, G., R. Kwok, and D. Menemenlis, 2011: Trends in Arctic sea ice drift and role of wind forcing: 1992–2009. *Geophys. Res. Lett.*, **38**, L19501, https://doi.org/10.1029/2011GL048970.

Stroeve, J., M. M. Holland, W. Meier, T. Scambos, and M. Serreze, 2007: Arctic sea ice decline: Faster than forecast. *Geophys. Res. Lett.*, **34**, L09501, https://doi.org/10.1029/2007GL029703.

Swart, N. C., J. C. Fyfe, E. Hawkins, J. E. Kay, and A. Jahn, 2015: Influence of internal variability on Arctic sea-ice trends. *Nat. Climate Change*, **5**, 86–89, https://doi.org/10.1038/nclimate2483.

Thorndike, A. S., 1992: A toy model linking atmospheric thermal radiation and sea ice growth. *J. Geophys. Res.*, **97**, 9401–9410, https://doi.org/10.1029/92JC00695.

Thorpe, S. A., 1998: Nonlinear reflection of internal waves at a density discontinuityat the base of the mixed layer. *J. Phys. Oceanogr.*, **28**, 1853–1860, https://doi.org/10.1175/1520-0485(1998)028<1853:NROIWA>2.0.CO;2.

Toole, J. M., R. A. Krishfield, M.-L. Timmermans, and A. Proshutinsky, 2011: The ice-tethered profiler: Argo of the Arctic. *Oceanography*, **24** (3), 126–135, https://doi.org/10.5670/oceanog.2011.64.

Vancoppenolle, M., T. Fichefet, H. Goosse, S. Bouillon, G. Madec, and M. A. M. Maqueda, 2009: Simulating the mass balance and salinity of Arctic and Antarctic sea ice. 1. Model description and validation. *Ocean Modell.*, **27**, 33–53, https://doi.org/10.1016/j.ocemod.2008.10.005.

Vavrus, S. J., and R. Alkama, 2022: Future trends of Arctic surface wind speeds and their relationship with sea ice in CMIP5 climate model simulations. *Climate Dyn.*, **59**, 1833–1848, https://doi.org/10.1007/s00382-021-06071-6.

Von Appen, W.-J., T. M. Baumann, M. Janout, N. Koldunov, Y.-D. Lenn, R. S. Pickart, R. B. Scott, and Q. Wang, 2022: Eddies and the distribution of eddy kinetic energy in the Arctic Ocean. *Oceanography*, **35** (3–4), 42–51, https://doi.org/10.5670/oceanog.2022.122.

Wagner, T. J. W., and I. Eisenman, 2015: How climate model complexity influences sea ice stability. *J. Climate*, **28**, 3998–4014, https://doi.org/10.1175/JCLI-D-14-00654.1.

Walker, G. T., 1931: On periodicity in series of related terms. *Proc. Roy. Soc. London*, **131A**, 518–532, https://doi.org/10.1098/rspa.1931.0069.

Weeks, W. F., and W. D. Hibler III, 2010: *On Sea Ice.* University of Alaska Press, 664 pp.

Weingartner, T., C. Ashjian, L. Brigham, T. Haine, L. Mack, D. Perovich, and B. Rabe, 2022: Introduction to the special issue on the new Arctic Ocean. *Oceanography*, **35** (3–4), 6–9, https://doi.org/10.5670/oceanog.2022.132.

Worster, M. G., and D. W. Rees Jones, 2015: Sea-ice thermodynamics and brine drainage. *Philos. Trans. Roy. Soc.*, **A373**, 20140166, https://doi.org/10.1098/rsta.2014.0166.

Yager, P. L., D. W. R. Wallace, K. M. Johnson, W. O. Smith Jr., P. J. Minnett, and J. W. Deming, 1995: The northeast water polynya as an atmospheric CO_2 sink: A seasonal rectification hypothesis. *J. Geophys. Res.*, **100**, 4389–4398, https://doi.org/10.1029/94JC01962.

Yule, G. U., 1927: VII. On a method of investigating periodicities disturbed series, with special reference to Wolfer's sunspot numbers. *Philos. Trans. Roy. Soc.*, **A226**, 267–298, https://doi.org/10.1098/rsta.1927.0007.

Zhang, Y., H. Wei, Y. Lu, X. Luo, X. Hu, and W. Zhao, 2020: Dependence of Beaufort Sea low ice condition in the summer of 1998 on ice export in the prior winter. *J. Climate*, **33**, 9247–9259, https://doi.org/10.1175/JCLI-D-19-0943.1.

Zhong, W., S. T. Cole, J. Zhang, R. Lei, and M. Steele, 2022: Increasing winter ocean-to-ice heat flux in the Beaufort Gyre region, Arctic Ocean over 2006–2018. *Geophys. Res. Lett.*, **49**, e2021GL096216, https://doi.org/10.1029/2021GL096216.